Accepted Version published in *Synthetic Metals* 10.1016/j.synthmet.2022.117030

Electrochemical Deposition of PEDOT/MoS_2 Composite Films for Supercapacitors

Alexey I. Volkov[a], Alexander V. Ivanov[a], Anatoliy A. Vereshchagin[a], Julia V. Novoselova[a], Elena G. Tolstopjatova[a], Veniamin V. Kondratiev[a]*

[a]Saint Petersburg State University, Universitetskaya nab. 7/9, Saint Petersburg, Russia 199304

*email: vkondratiev@mail.ru

Abstract

Composite materials based on conducting polymers and transitional metal chalcogenides have attracted considerable attention as electrode materials for supercapacitors. Molybdenum disulfide is a layered transitional metal dichalcogenide extensively researched in energy storage and conversion applications, and poly(3,4-ethylenedioxythiophene) (PEDOT) is an intrinsically conducting polymer that can act as a conductive matrix. We propose a single-step electrochemical deposition of PEDOT/MoS_2 composite materials from the dispersion containing commercially available MoS_2 platelets and EDOT monomer. Potentiodynamic, galvanostatic, and potentiostatic modes are all suitable for synthesis of the materials with predominant content of MoS_2, which is attached to the current collector via conducting PEDOT matrix. The materials can work in various water-based electrolytes and combine capacitor-like and redox pseudocapacitive response. The composites deposited on graphite foil in assembled asymmetric cells with Kynol carbon cloth counter-electrode deliver up to 870 mF cm^{-2} areal capacitance in $LiClO_4$ aqueous solution at a current density of 1 mA cm^{-2} due to combined capacitive input of both components.

Keywords

molybdenum disulfide; PEDOT; supercapacitors; composite film electrode; areal capacitance; electrochemical synthesis.

1 Introduction

The demand for green and reliable chemical energy storage devices has increased drastically in recent years. Supercapacitors are one of the desired options due to their high charge-discharge rates and cyclic stability. There are three types of supercapacitors depending on charge storage mechanism within the electrodes [1]. Electrochemical double-layer capacitors (EDLC) (1) store and provide energy by charging the double layer. Pseudocapacitive capacitors (2) store charge via fast faradaic processes. Electrode materials in these usually consist of conducting polymers or transition metals oxides, which undergo highly reversible redox processes in the film electrodes. Hybrid supercapacitors (3) combine both types of charge storage mechanisms.

Two-dimensional layered nanomaterials are widely considered as candidates for pseudocapacitive charge storage. Their main advantage is the graphene-like layered structure that both enhances electrolyte access along the surface planes and provides mechanical stability. Such materials can effectively store energy by recharging the redox centers, and their layered structure provides higher specific surface area and facilitates surface electron transfer and injection of counter-ions into the crystal structure. Transmission metal dichalcogenides, such as molybdenum disulfide, belong to such materials [2–5].

Molybdenum disulfide attracts attention because of its high theoretical capacitance and relatively low cost. MoS_2 can store charge effectively due to pseudocapacitance in positive range of potentials [6], and double layer capacitance

in the negative one [7]. Thus, it may act both as cathode and anode material for supercapacitors. However, its application is hindered by low reversible capacitance and cycle life. The main reasons of these drawbacks are low electronic conductivity, structural reorganization, and volumetric changes during cycling, which result in isolation of MoS_2 active particles. Two main strategies to overcome this problem exist: changing the morphology of MoS_2 or obtaining nanocomposites [5,8–11], including those with conducting polymers [4,12–21].

Metallic centers in MoS_2 provide strong association with nitrogen and sulfur atoms in conducting polymers (e.g., poly(3,4-ethylenedioxythiophene), polyaniline, polypyrrole), which contributes to growth of conducting polymers on the MoS_2 surface. The composites based on conducting polymers and 2D-materials exhibit electrochemical properties of both components via the synergetic effect owing to enhanced charge transport between these two components.

In addition to enhancement of transport properties of composite materials, conducting polymers can store charge themselves. Favorable properties of PEDOT include fast redox reactions, good charge-discharge properties and stable conductivity in a wide range of potentials. Thus, PEDOT is a viable electrode material in various electrolyte solutions [22]. A distinct feature of PEDOT is ability to form very thick (up to 0.5 mm) films via electrochemical synthesis. Electrochemically obtained films are micro- and nanoporous and retain their charge-discharge properties. Specific capacitance of PEDOT films grows linearly along with the film deposition charge and can reach up to 0.46 F cm^{-2} in composites with carbon nanotubes [23].

Thus, combination of inorganic materials with conducting polymers is a prospective method of obtaining materials for supercapacitors with high capacities. There are reports on synthesis and study of MoS_2/PANI [12], MoS_2/PPy [14,15],

and MoS_2/PEDOT or MoS_2/PEDOT:PSS [13,16–22,24,25] composites. Composite PEDOT/MoS_2 materials based on MoS_2 nanolayers can be synthesized both via in situ oxidative EDOT polymerization [16,17,19] and via electrochemical polymerization [13,21,25].

In this work, we present the method of MoS_2 electrochemical deposition into PEDOT matrix with formation of MoS_2/PEDOT composite using a special upside-down electrochemical cell. This method of synthesis employs a dispersion of commercially available MoS_2 within EDOT acetonitrile solution, which allows to deposit the composite via MoS_2 trapping within electropolymerized PEDOT matrix. Composition, structure and morphology of MoS_2/PEDOT composites were characterized using spectral methods. Electrochemical studies of the composites were performed in a series of aqueous electrolytes. The composites were then synthesized on graphite foil and studied using cyclic voltammetry and galvanostatic charge-discharge methods in an asymmetric cell with carbon cloth electrode.

2 Experimental

2.1 Materials

MoS_2 nanopowder (90 nm, 99%), 3,4-ethylenedioxythiophene (EDOT) (97%), tetrabutylammonium tetrafluoroborate (Bu_4NBF_4) (99%), $LiClO_4$ (99%) were obtained from Aldrich, acetonitrile (HPLC grade) was obtained from abcr, KCl (>99%) and Li_2SO_4 (98%) were obtained from Reachem, H_2SO_4 was obtained from Neva-Reaktiv. Glassy carbon electrode (S=0.283 cm^2) was polished with alumina powder before each use. Graphite foil was cut into 1 cm^2 squares. Deionized water (>18 MΩ cm resistivity) was obtained using Millipore DirectQ UV water purification system.

2.2 Synthesis

Electrochemical synthesis of composites was conducted differently depending on the used conductive substrate. For glassy carbon working electrode, an upside-down electrochemical cell was assembled, in which the glassy carbon electrode was placed facing upwards. A plastic tube was tightly connected to the electrode and served as an electrolyte vessel. Pt and Ag wires served as a counter and a reference electrodes, respectively. The solution for synthesis was prepared by dissolving 0.06 mol dm^{-3} EDOT and 0.05 mol dm^{-3} Bu_4NBF_4 in acetonitrile, followed by addition of 0.03 mol dm^{-3} of MoS_2 particles [13]. The resulting dispersion was sonicated for 15 min immediately prior to synthesis to agitate the dispersion and prevent the formation of MoS_2 agglomerates. The dispersion was added into the upside-down cell. The position of the working electrode supposed that the composite deposition would be assisted by sedimentation in addition to electrodeposition.

Composite films were then immediately synthesized using potentiodynamic or galvanostatic deposition mode as per Scheme 1. Autolab PGSTAT30 (Metrohm), Interface1000 (Gamry Instruments) and Elins P-40X (Electrochemical Instruments) potentiostats was used for synthesis and characterization. In potentiodynamic mode, the potential was cycled in -1.2 V to 1.3 V (vs. Ag/AgCl) for 10 cycles at 0.1 V s^{-1} scan rate. In galvanostatic mode, the composites were synthesized for 2000 s at 1 mA cm^{-2} current density.

For comparison, PEDOT electrodes without MoS_2 were prepared separately from 0.06 mol dm^{-3} EDOT and 0.05 mol dm^{-3} Bu_4NBF_4 solution in acetonitrile in both potentiodynamic and galvanostatic modes with the same parameters.

After synthesis, the electrodes were washed with deionized water and dried in air for 2 h at 60 °C.

The suitability of materials as supercapacitor electrodes was studied for composites deposited on graphite foil (1 cm^2) samples. In this case, during electrodeposition, synthesis solution was constantly stirred with a magnetic stirrer to maintain the stability of the MoS_2 suspension. One synthesis cycle consisted of potentiostatic deposition at 1.1 V, followed by 10 min air drying, and each synthesis consisted of five such cycles. Afterwards, the electrodes were air-dried, carefully rinsed with water, and then dried for 1 h in a vacuum. Mass loadings of the cathode materials were determined by direct weighing to comprise ca. 6.5 mg cm^{-2}.

2.3 Electrochemical characterization

The properties of composites on glassy carbon electrodes were investigated in various aqueous electrolytes (1 mol dm^{-3} KCl, 1 mol dm^{-3} $LiClO_4$, 0.5 mol dm^{-3} Li_2SO_4, 0.5 mol dm^{-3} H_2SO_4). Standard three-electrode cell was used with working electrode with either PEDOT/MoS_2 composite or PEDOT film, Pt foil as counter electrode, and Ag/AgCl (sat. NaCl) as reference electrode. Cyclic voltammetry measurements were conducted in various ranges to determine the effect of potential windows (in the total range of -0.9 V to 1.3 V) at scan rates from 0.005 V s^{-1} to 0.5 V s^{-1}.

Cell prototypes were assembled with obtained graphite foil electrodes using a custom-designed holder made of PTFE, Kynol carbon cloth as the counter electrode, a polypropylene separator, and stainless-steel current collectors (Scheme 2). Kynol was selected as it can be used as an electrode in EDLC [26]. For these tests, 1 mol dm^{-3} $LiClO_4$ aqueous electrolyte was used. Ag/AgCl (sat. NaCl) was used as reference electrode. Thus, an asymmetric hybrid supercapacitor was assembled, and reference electrode allowed for a more precise control of potential. Cyclic voltammetry measurements were conducted at various scan rates from 5 mV s^{-1} to 100 mV s^{-1}, and various potential windows were studied. Galvanostatic

charge-discharge curves at current densities from 1 mA cm^{-2} to 10 mA cm^{-2} were recorded in symmetric mode to obtain specific capacity values.

Electrochemical impedance spectra of both pristine PEDOT film and PEDOT/MoS_2 composite were obtained in 20 kHz to 10 mHz frequencies range with 5 mV rms amplitude for the open-circuit potential. The spectra were fitted using Autolab Nova 2.1.5 software, with $\chi^2 \leq 0.01$ for the obtained values.

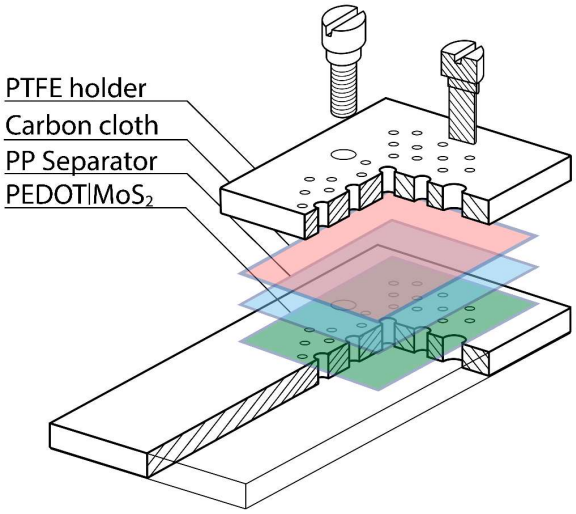

Scheme 1. The cell used for the studies of PEDOT/MoS_2 composite deposited on graphite foil.

The data were plotted and analyzed using and OriginPro software. Perceptually uniform scientific color map *batlow* [27] was used to prevent visual distortion of the data and exclusion of readers with color vision deficiencies [28].

2.4 Morphology and structure investigation

The morphology of materials synthesized on glassy carbon substrate was studied with scanning electron microscopy (SEM) (SUPRA 40VP Carl Zeiss, Germany) and transmission electron microscopy (TEM) (Zeiss Libra 200FE). The elemental composition was analyzed using energy-dispersive X-ray spectroscopy (SUPRA

40VP Carl Zeiss, Germany). X-ray diffraction (XRD) (Bruker-AXS D8 DISCOVER, Cu-Kα, λ=0.15406 nm) was used to determine the structure of MoS2. X-ray photoelectron spectroscopy (XPS) (Thermo Fisher Scientific Escalab 250Xi) allowed to determine the valence states of elements present in composite samples.

3 Results and discussion

3.1 Electrochemical deposition

Under intensive stirring in aqueous and organic solutions, medium-sized MoS_2 particles form poorly stable dispersions that quickly settle. This condition of rapid sedimentation renders traditional methods of electrochemical synthesis ineffective because vertically immersed working electrodes do not provide enough area for capturing of sufficient number of particles during electrochemical polymerization. To solve such problems, we have previously developed an original synthesis method and design of an electrochemical cell with a working electrode occupying most of its bottom [29,30], which can be used for one-step template synthesis (Scheme 1).

During electrodeposition in such cell, two parallel processes take place: sedimentation of finely dispersed solid MoS_2 particles on the electrode surface, on which the conducting polymer layer is building up, and propagation of the electrochemically synthesized PEDOT polymer through the space between the settled particles, binding the precipitate into a composite film. Thus, in the synthesis of a PEDOT/MoS_2 composite film, the MoS_2 precipitate serves as a matrix for PEDOT growth. This method of electrochemical deposition provides a network of interconnected MoS_2 particles with multiple exposed facets firmly attached to the current collector by the PEDOT film forming a nanostructured material with nanosized precipitate particles distributed throughout the volume of the composite electrode.

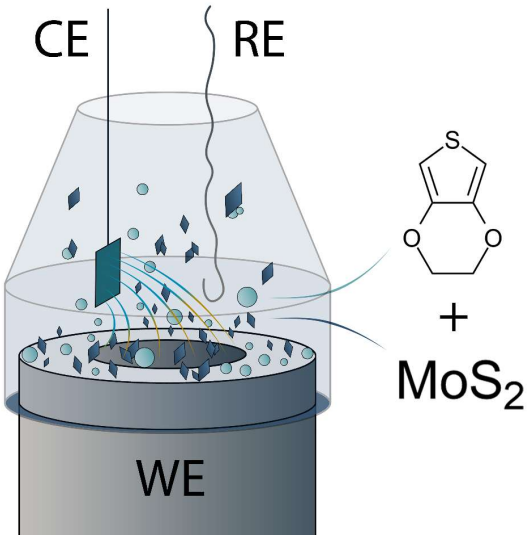

Scheme 1. The cell used for synthesis of composite electrode material on glassy carbon (WE) with Pt counter electrode (Pt) and Ag pseudo-reference electrode (RE).

Electrochemical templating synthesis of PEDOT/MoS_2 composites on glassy carbon electrodes was performed in potentiodynamic and galvanostatic modes. Pristine PEDOT film was synthesized separately using the same procedure for comparison.

During 10 cycles of potentiodynamic synthesis (Figure 1a), a uniform increase of CV current was observed. Two peaks at potentials of about -0.2 V and 0.4 V are observed on the anodic branch of the CV, while cathodic branch contains a peak at -0.8 V, and a weakly pronounced peak at ca. 0.25 V. Similarly, the observed form of PEDOT deposition CV (Figure 1b) is characteristic of the electrochemical response of PEDOT films in organic electrolytes [31,32], and contains an anodic peak at 0.2 V, and two cathodic peaks at 0.1 V and -0.6 V. As there is no anodic peak at 0.4 V during PEDOT deposition, it can be attributed to the oxidation of deposited MoS_2 particles. The initially present pair of peaks at ca. -0.8 V (oxidation) / -1.0 V (reduction) quickly disappears after 3 cycles and may be

related to initial adsorption-desorption of species containing in the electrolyte, as n-doping processes of PEDOT itself usually occur in more negative potential range [32].

Generally, the deposition of PEDOT/MoS_2 is accompanied by faster increase of electrochemical activity, than in the case of analogous deposition of pristine PEDOT film. Such difference is largely due to the capture of MoS_2 platelets in the composite film, and the resulting capacitance is a superposition of PEDOT non-faradaic and MoS_2 redox capacitance.

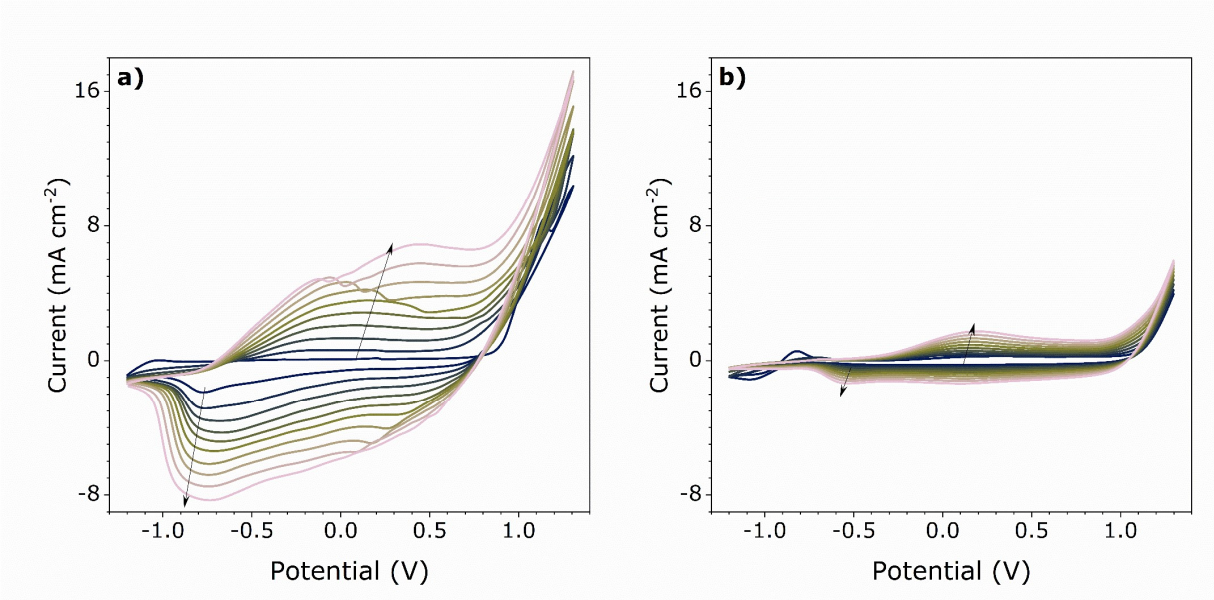

Figure 1. Potentiodynamic electrodeposition curves for (a) PEDOT/MoS_2 composite and (b) PEDOT film on glassy carbon electrode.

3.2 Structure and morphology

Pristine MoS_2 (Figure 2a) powder consists of multiple layered platelets with 100 nm to 400 nm lateral sizes, with the ~10 nm thickness of individual layers. SEM image of the sample deposited potentiodynamically on the surface of glassy carbon (Figure 2b) shows that the polymer makes up the layer immediately adjacent to the current collector, with the thickness of ca. (400–550) nm. The rest

of the material (Figure 2c) is composed of multiple disorganized MoS_2 platelets on the surface of PEDOT, amounting to the thickness of ~5 μm (Figure S2). As the composite does not peel off, and its integrity can only be disturbed mechanically (e.g., scratching) the external layer of MoS_2 must be attached to the current collector via the deposited polymer. Multiple exposed facets of the material can thus provide increased internal surface area beneficial for capacitive properties.

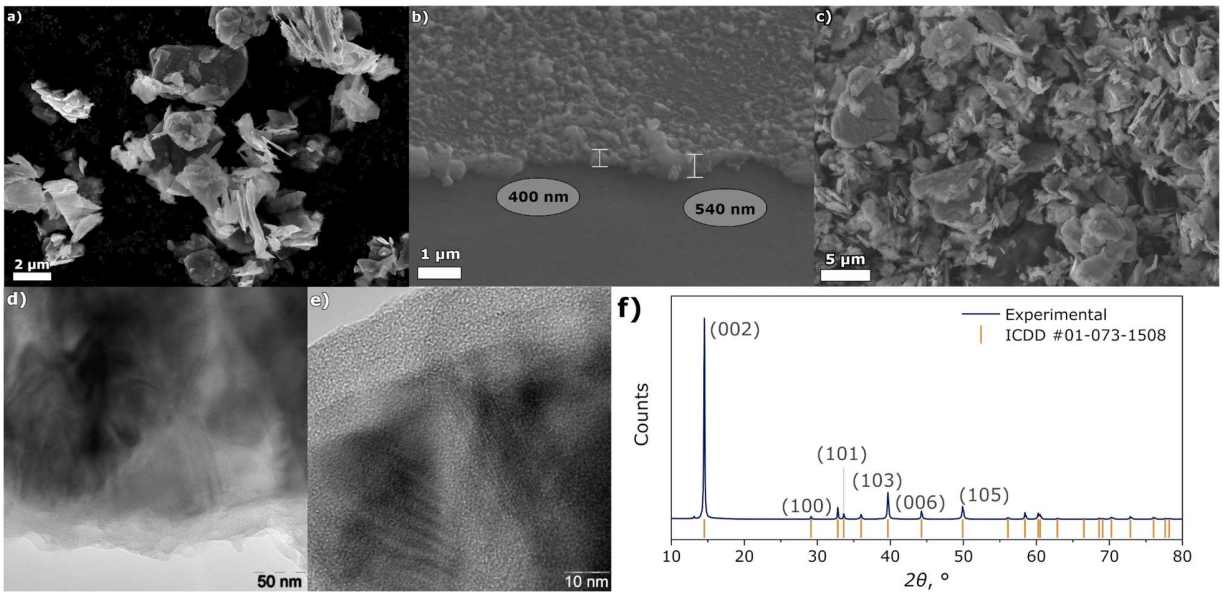

Figure 2. SEM images of a) pristine MoS_2 powder, b) edge of the PEDOT/MoS_2 composite film at 45° showing polymer thickness, c) the surface of PEDOT/MoS_2 composite film; d, e) TEM images of MoS_2 platelets embedded into PEDOT at various magnifications; f) XRD spectrum of pristine MoS_2 powder.

At lower magnification (Figure 2d), TEM images contain distinctive Moiré fringes, as the deposited platelets are multilayered. The edges of layers are also visible. Image at higher magnification (Figure 2e) shows clear hexagonal patterns of the deposited MoS_2 layers. The layered structure should allow for better surface availability of MoS_2 platelets, increasing double-layer capacitance of the composite.

The XRD pattern of MoS_2 used in this work (Figure 2f) matches that of semi-conductive 2H-MoS_2 (P83/mmc space group), ICDD # 01-073-1508 [33]. Low full width at half maximum values of peaks indicates high crystallinity of the sample, while (103) and (105) signals are related to the multilayered structure of MoS_2 particles [34].

EDX analysis and elemental mapping for the composites (Figure S1) shows the high prevalence of MoS_2 compound in the obtained composites, as the signals related to Mo and S elements are more intense than those of C and O, which could be attributed to PEDOT. The exact ratio is difficult to estimate, considering the overlap between Mo and S signals. The additional images obtained after continuous cycling (Figure S3) show that material preserves its structure of multiple MoS_2 platelets embedded into the PEDOT matrix without significant pulverization, amorphization or aggregation of the material.

XPS measurements (Figure S4) have shown that the expected S, Mo, C and O elements are present in the obtained material (Figure S1a), and the spectra are generally consistent with reported for similar composite [25]. The S 2p peaks at 168.4 eV, 163.4 eV and 162.2 eV are assigned to S^{4+}, C-S bond, and S $2p_{3/2}$, respectively, where C-S signal originates from PEDOT.

3.3 Electrochemical properties

The charge storage mechanism for PEDOT films is pseudocapacitive and is represented by the following scheme of electrochemical doping/dedoping of the polymer:

$$PEDOT_n^0 - e^- \overset{+A^-,\ xSol}{\rightleftarrows} [(PEDOT^{+\cdot})A^- \cdot xSol]_n \qquad \text{Eq. (1)}$$

In aqueous solutions, PEDOT films show nearly rectangular CVs (Figure 3) without distinct anodic or cathodic peaks. For all synthesized films, areal

capacitance of PEDOT is 64±4 mF cm^{-2}. PEDOT/MoS_2 films show a major increase of capacitance, from 4.5 to 6.5 times as much as PEDOT films depending on the selected solution. The highest specific capacitance of 405 mF cm^{-2} is shown for 1 mol dm^{-3} KCl solution (Figure 3a). The areal capacitance at a scan rate of 10 mV s^{-1} of the composite is 274 mF cm^{-2}, 374 mF cm^{-2}, and 227 mF cm^{-2} for $LiClO_4$, Li_2SO_4, and H_2SO_4 solutions, respectively. PEDOT/MoS_2 composite films in aqueous electrolytes show distinct features depending on the selected solution. The CVs retain their pseudocapacitive rectangularity, yet in KCl, Li_2SO_4 and H_2SO_4 electrolytes a pair of peaks appears. For KCl electrolyte, the oxidation and reduction peaks are at 0.23 V and -0.06 V, and the same pair is at 0.20 V and -0.12 V for Li_2SO_4 (Figure 3c). In H_2SO_4 (Figure 3d), likely due to pH, the peaks shift to 0.51 V and 0.11 V. As these peaks only arise in the case of composite, they are most likely related to MoS_2 component. The most intense pair of peaks is in the case of KCl, which may be due to lower charge density of the K^+ ion, allowing for less disruptive intercalation between the layers of MoS_2. The remaining electrolyte, $LiClO_4$ (Figure 3b), shows nearly flat current response in the potentials range from -0.3 V to ca. 0.6 V, which is beneficial for use in supercapacitor applications. Regardless of the choice of electrolyte, for PEDOT/MoS_2 a current increase is observed at >0.6 V potentials. As this response is reproducible during continuous cycling, it is not due to degradation of the material, but rather due to transformation of MoS_2 and appearance of Mo^{6+} forms detected by XPS method at 235.7 eV (Figure S4).

The rectangular shape of the CVs in the case of PEDOT/MoS_2 composite is due to non-faradaic process of MoS_2 charging, i.e., the capacitance resulting from the charging of the layer via adsorption of protons or cations on the surface of MoS_2:

$$(MoS_2)_{surface} + C^+ + e^- \rightleftarrows (MoS_2^- - C^+)_{surface} \qquad \text{Eq. (2)}$$

Another mechanism inherent to layered materials, such as MoS_2, is due to capability of dynamic expansion of interlayer distance, that allows insertion of alkali metal ions, present in the electrolyte, in between material layers, according to the following scheme:

$$MoS_2 + C^+(Na^+, Li^+, K^+, H^+) + e^- \rightleftarrows MoS - S(C^+) \qquad \text{Eq. (3)}$$

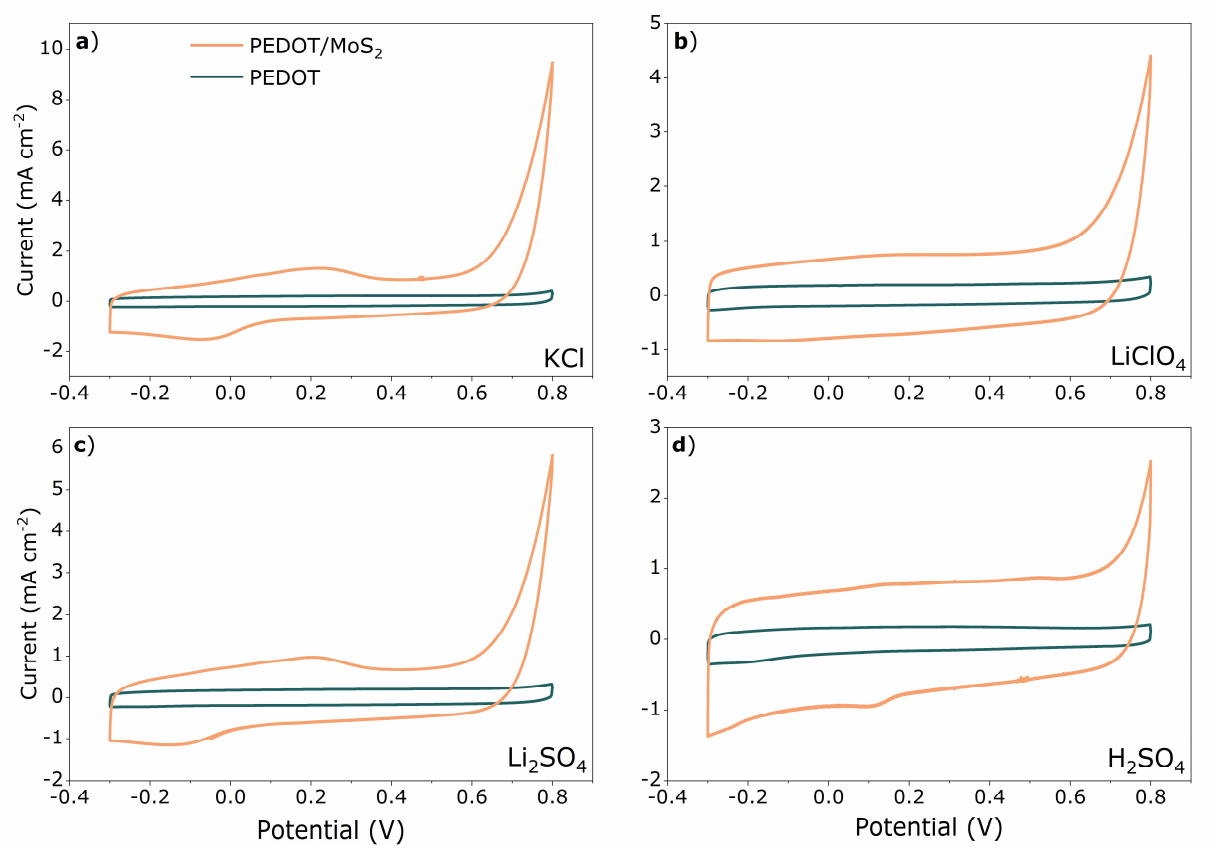

Figure 3. CVs of PEDOT/MoS_2 composite at 0.01 V s^{-1} in a) 1 mol dm^{-3} KCl, b) 1 mol dm^{-3} $LiClO_4$, c) 0.5 mol dm^{-3} Li_2SO_4, and d) 0.5 mol dm^{-3} H_2SO_4 aqueous solutions. CVs of pristine PEDOT films obtained in the same conditions are provided for reference.

At lower scan rates (Figure 4a,b), this redox-process involving molybdenum is responsible for emergence of the CV peaks [3]. Such pseudocapacitive response due to ions intercalation was reported for MoS_2 films, and appearance of additional peaks is accompanied by an overall increase of current [3,8,10].

The processes related to the anodic peak during MoS_2 oxidation are sensitive to the material structure (particles size) and the medium [35,36]. The larger the particles are, the later the oxidation onsets. Upon reaching the oxidized state at >0.5 V (Figure 4a), a reduction process emerges at -0.1 V. Thus, in anodic process, Mo^{4+} oxidized to Mo^{6+}, which leads to emergence of anodic wave, then Mo^{6+} reduces back to Mo^{4+} in the reverse process. In a more negative potentials area, capacitive behavior is also prevalent (Figure 4b). Still, there is a slight peak at potentials of -0.75 V to -0.68 V, depending on the selected electrolyte, related to PEDOT oxidation/reduction [37]. The only obvious exception is 0.5 mol dm^{-3} H_2SO_4 electrolyte, where H_2 evolution occurs at potentials <-0.4 V, which is common in low-pH media.

At higher scan rates (Figure 4c,d) the Faradaic processes are not as noticeable as capacitive response of the material becomes predominant even in higher potentials range. This is expected, as surface-located processes (Eq. 1 and Eq. 2) contribute more at faster rates, than interlayer interactions (Eq. 3). The electrolyte based on $LiClO_4$ maintains near-rectangular shape of the CV response both at low and high scan rates, which makes it a suitable candidate for application in supercapacitors. Unlike a 2:1 electrolyte Li_2SO_4, lithium ions do not contribute significantly to intercalation processes.

CVs for both low and high scan rates for a more negative potentials area show (Figure 4b,d) that at <-0.8 V the composite has very low electrochemical activity, likely due to PEDOT being in non-conducting state.

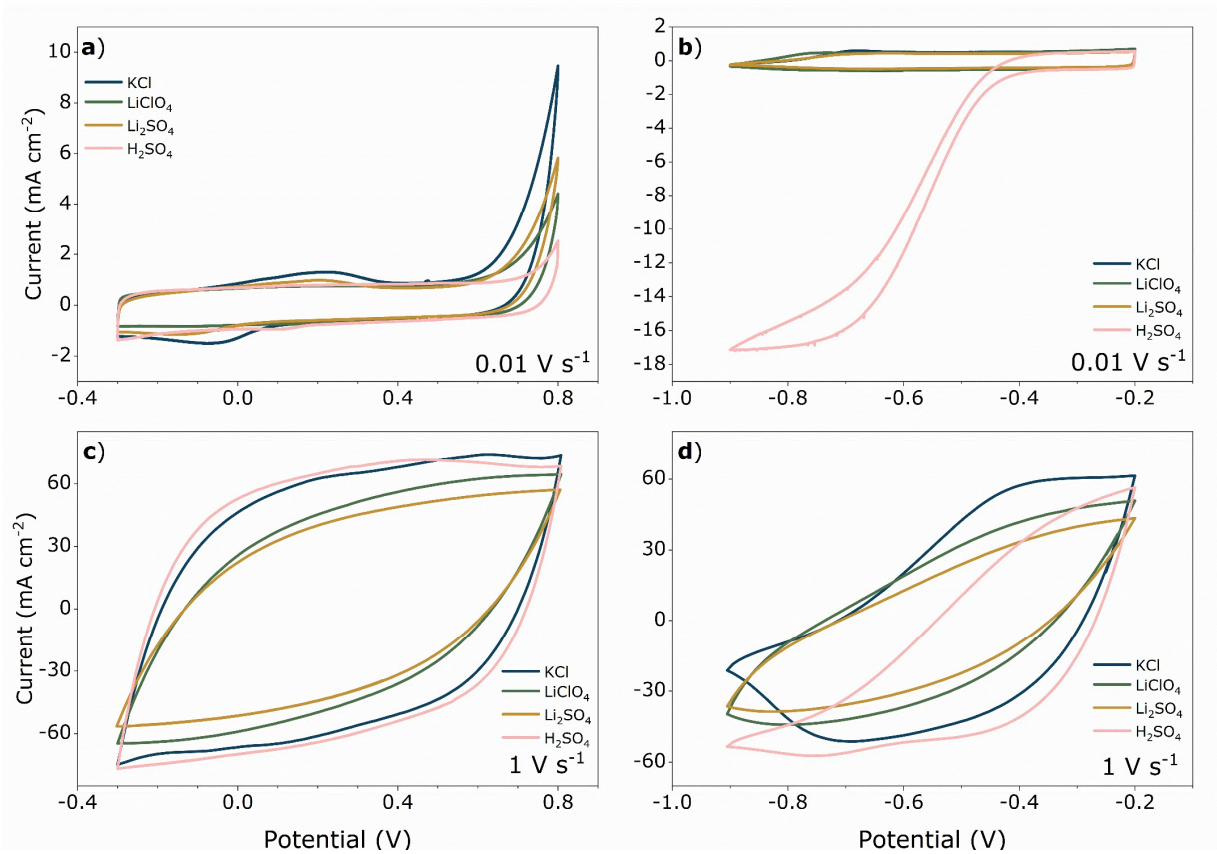

Figure 4. Cyclic voltammograms of PEDOT/MoS_2 composites at low (0.01 V s^{-1}) (a, b), and high (0.1 V s^{-1}) (c, d) scan rates in various electrolytes in negative (a, c) and positive (b, d) potential windows.

Hydrogen evolution reaction in 0.5 mol dm^{-3} H_2SO_4 when cycled in -0.9 V to -0.2 V potentials range makes it an undesirable electrolyte for further application (Figure 4b). The remaining electrolytes are suitable for use of PEDOT/MoS_2 composites in lower potentials area, as the areal capacitance is 105 mF cm^{-2} in KCl, 108 mF cm^{-2} in $LiClO_4$, and 87 mF cm^{-2} in Li_2SO_4. Here, $LiClO_4$ electrolyte provides the highest capacitance value, though at a higher scan rate of 1 V s^{-1}, the material performs best in 1 mol dm^{-3} KCl solution with 79 mF cm^{-2} capacitance. Leaf-like shape of CVs deteriorates at 1 V s^{-1} in negative potentials area (Figure 4d), which ultimately decreases total capacitance and may effectively lead to decrease of the cycling window. Yet, the presented potential areas show that the

material exhibits stable performance in 1.1 V potential window both in negative and positive ranges.

To study the effects that the potential range, especially its upper limit, brings to electrochemical performance of PEDOT/MoS_2 and the shape of CVs, the upper potentials area was variated. 0.5 mol dm^{-3} Li_2SO_4 was selected, as the film capacity was relatively high there, and the shape of CV (Figure 5) allowed to see both adsorption capacity and faradaic pseudo capacity.

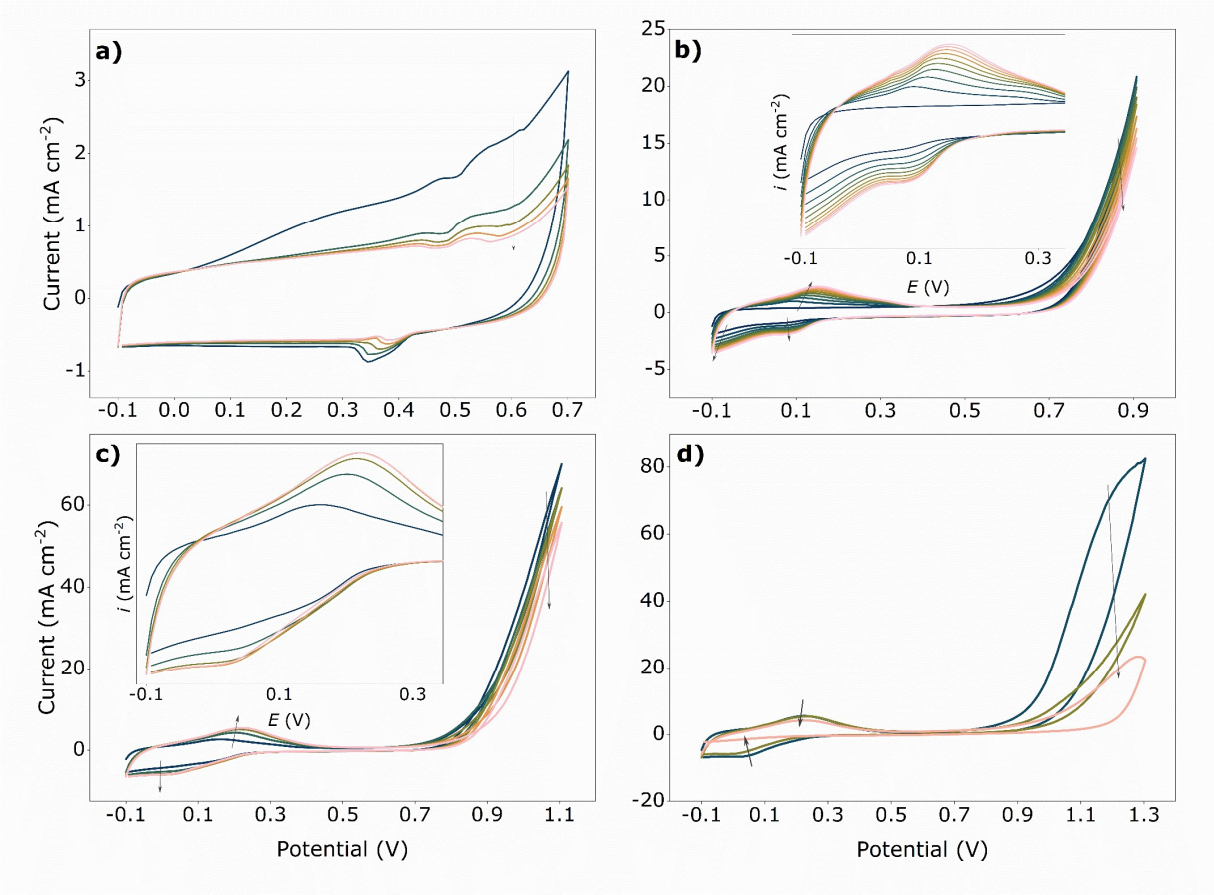

Figure 5. Cyclic voltammograms of PEDOT/MoS_2 composite in 0.5 mol dm^{-3} Li_2SO_4 in with varying potential windows at 0.01 V s^{-1}. a) (-0.1–0.7) V, b) (-0.1–0.9) V, c) (-0.1–1.1) V, d) (-0.1–1.3) V.

First, the film was continuously cycled in the -0.1 V to 0.7 V potentials range (Figure 5a). At the first cycle, currents noticeably higher than those of the stable film

response are observed (the "first cycle effect" associated with the transition of the material from the equilibrium state to its active form). A quasi-rectangular shape of the CVs is visible here, and a pair of peaks at 0.53 V and 0.34 V becomes visible. They are related to MoS_2 redox processes. As these peaks are relatively low, the main contribution to capacitance is combined pseudocapacitive response from PEDOT and double-layer capacitance of MoS_2.

Upon the increase of the cycling range to 0.9 V (Figure 5b), a pronounced anodic wave at potentials >0.7 V arises with a slight decrease in currents during continuous cycling. At the same time, an increase in currents of cathodic and anodic peaks at negative potentials was observed (Figure 5b inset). Similar dependences were observed when the cycling range was further increased up to 1.1 V (Figure 4c), which lead to an even higher increase of peak currents. This is the highest available cycling range for these films, as further increase of potentials range up to 1.3 V (Figure 5d) led to a rapid drop in the currents, which is primarily attributed to the degradation of PEDOT [38,39].

Comparison of the specific capacitances of the PEDOT/MoS_2 composite obtained from CVs recorded for the same film at different potential ranges showed that in the case where only charging of the MoS_2 double-layer capacitance occurs the achieved values of specific capacitance are moderate (~57 mF cm^{-2}). Upon extension of the cycling range, the redox processes involving molybdenum ions contribute significantly to the pseudocapacitive component of the composite total capacitance, which allows to achieve a tenfold increase in the specific capacitance of the PEDOT/MoS_2 composite film. Thus, when cycling the potential of the PEDOT/MoS_2 film within -0.1 V to 1.1 V potentials range, the specific capacitance reaches 650 mF cm^{-2}.

Galvanostatic synthesis of PEDOT/MoS_2 films was done at j=1 mA cm^{-2} from the same synthesis solution as in the case of potentiodynamic synthesis. During 2000 s of synthesis, the potential was ~(1.05—0.95) V. The dependency of potential on time was as reported before for PEDOT films [40].

The potential range stability of the film was also tested in Li_2SO_4 (Figure 6) to find similarities between composites obtained by two modes of synthesis. The general shape and the positions of peaks are the same as for films obtained potentiodynamically. Higher current values are a direct consequence of longer synthesis time and higher total charge passed. Narrower potentials range, -0.3 V to 0.8 V, shows anodic process onset at >0.6 V, and a slight increase of cathodic currents in consequent cycles at ~-0.2 V. The specific capacitance of the composite was 195 mF cm^{-2}, while for pristine PEDOT film a value of 80 mF cm^{-2} was obtained. The increase of the positive potential limit to 1.0 V led to the emergence of a more intense anodic wave, likely related to further oxidation of molybdenum to $^{+6}$ valence state, which existence has been shown in similar materials.[24] This caused the appearance of redox peaks at 0.05 V and 0.25 V, which may represent the change between Mo^{4+} and Mo^{3+} valence states.[41] The currents and total capacitance increased along with the cycle number, reaching 793 mF cm^{-2} on the 5th cycle already.

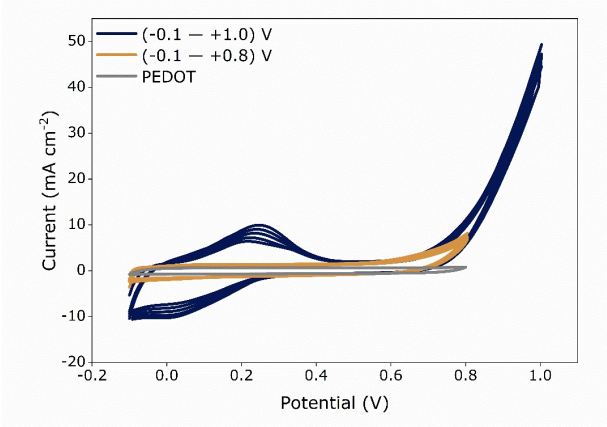

Figure 6. Cyclic voltammograms at 0.01 V s^{-1} in 0.5 mol dm^{-3} Li_2SO_4 of galvanostatically synthesized PEDOT/MoS_2 composite in two potential windows, and comparison to pristine PEDOT film synthesized in the same conditions.

To study the possibility of using the material on a current collector that could be assembled in a device, electrochemical tests were performed using the PEDOT/MoS_2 composite potentiostatically deposited on graphite foil in a cell construction depicted in Scheme 2. Here, we selected 1 mol dm^{-3} $LiClO_4$ electrolyte, as it is a 1:1 electrolyte that provided near-rectangular CV response in initial studies. First, the cell was cycled individually in positive and negative potential ranges (Figure 7a). As with glassy carbon, the positive potential range proved to be more beneficial for charge storage, yielding 384 mF cm^{-2} vs 291 mF cm^{-2} in a negative range at a scan rate of 5 mV s^{-1}. The major difference from the thin films deposited on glassy carbon substrate is a greater decrease of electrochemical activity at higher scan rates, which is likely due to higher resistance of the material in this case. This is especially visible from a leaf-shaped CV in full potentials range (Figure 7b). Still, the material provides up to 470 mF cm^{-2} in this case, in a total potential window of 1.7 V.

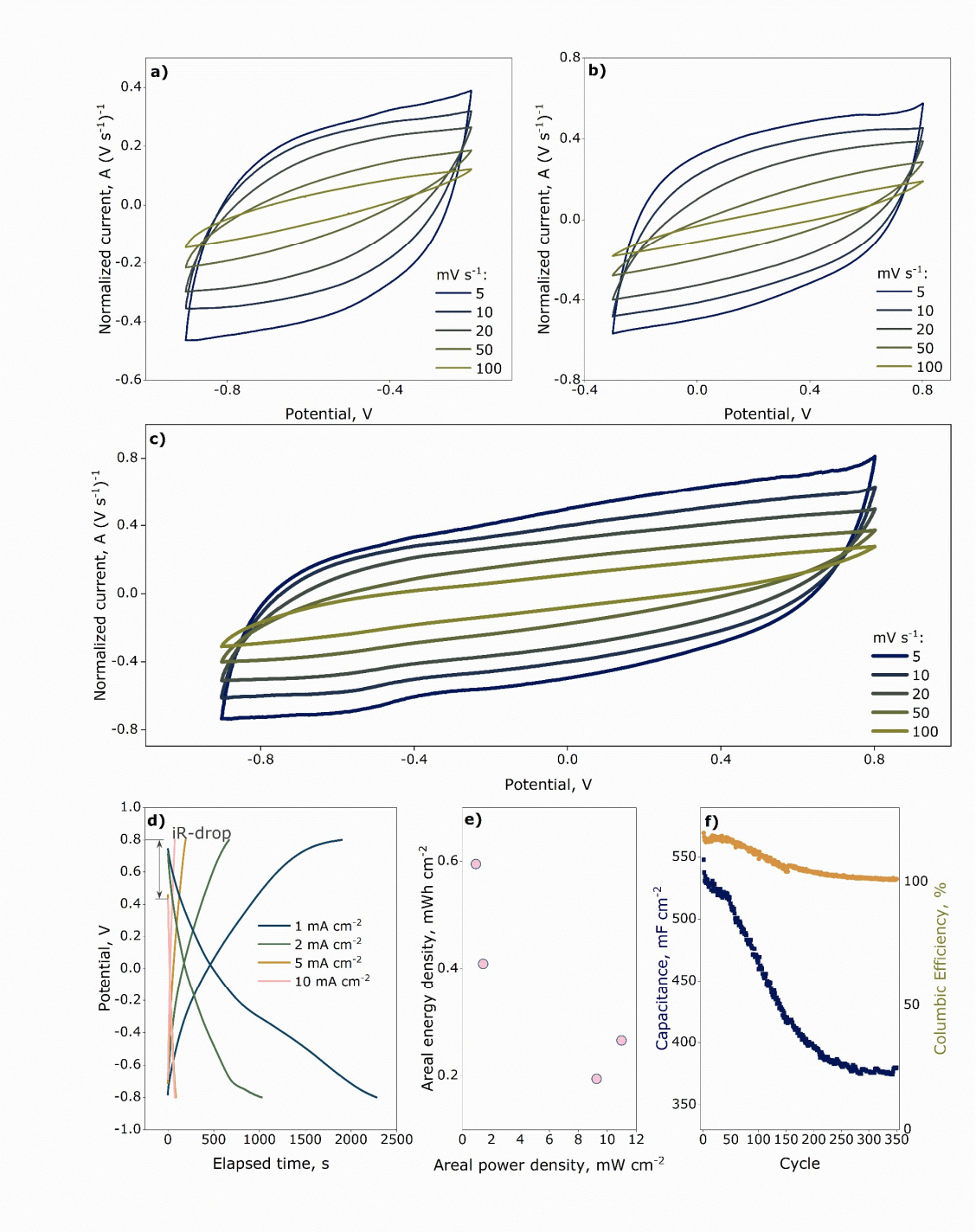

Figure 7. Electrochemical studies of PEDOT/MoS_2 composite in 1 mol dm^{-3} $LiClO_4$, deposited on 1 cm^2 graphite foil. CVs in a) (-0.9 – -0.2) V, b) in (-0.3–0.8) V potential ranges, c) in full (-0.9–0.8) V potential range. d) Galvanostatic charge-discharge curves at various current densities, e) areal energy and power densities for the material, f) cyclic stability at 5 mA cm^{-2}.

For galvanostatic charge-discharge tests (Figure 7c), the lower potential value was narrowed to -0.8 V to avoid possible hydrogen evolution. On discharge, the potential window was of 1.6 V was almost completely utilized in the cases of low current densities, yet at higher current rates the iR-drop limited that window. For 1 mA cm^{-2}, 2 mA cm^{-2}, 5 mA cm^{-2}, and 10 mA cm^{-2}, the potential drop values are 0.06 V, 0.09 V, 0.24 V, and 0.27 V, respectively. The material provided 903 mF cm^{-2} (139 F g^{-1}) at a current density of 1 mA cm^{-2}, 646 mF cm^{-2} (99 F g^{-1}) at 2 mA cm^{-2}, 517 mF cm^{-2} (80 F g^{-1}) at 5 mA cm^{-2}, and 396 mF cm^{-2} (61 F g^{-1}) at 10 mA cm^{-2}. These values correspond to the areal energy densities of 0.59 mWh cm^{-2}, 0.41 mWh cm^{-2}, 0.27 mWh cm^{-2}, and 0.19 mWh cm^{-2} at 0.94 mW cm^{-2}, 1.44 mW cm^{-2}, 11.0 mW cm^{-2}, and 9.27 mW cm^{-2}, respectively (Figure 7e), which are equivalent to gravimetric properties 92 Wh kg^{-1}, 63 Wh kg^{-1}, 41 Wh kg^{-1}, and 30 Wh kg^{-1} at power densities of 0.14 W kg^{-1}, 0.22 W kg^{-1}, 1.69 W kg^{-1}, and 1.43 W kg^{-1}, respectively.

The curves with near-constant slope are beneficial for use in capacitors, as constant current can be delivered. The lower potentials area may be a subject to further narrowing, as this area is responsible for increased coulombic efficiency at initial cycles. However, we show that during prolonged cycling the material coulombic efficiency stabilizes near 100%, as secondary processes recede (Figure 7f). The material cycled at 5 mA cm^{-2} delivers 87% of initial capacitance after 100 cycles, and 71% after 350 cycles. However, by the 250^{th} cycle the capacity is 286 mF cm^{-2}, and after additional 100 cycles, only 0.3% of capacitance is lost, which makes the material suitable for prolonged cycling after an initial drop of capacitance.

Electrochemical impedance spectroscopy (Figure 8) studies serve as additional confirmation of the composite enhanced performance. The data show that the composite has slightly lower charge transfer resistance (R_{ct}): 19.3 Ω versus 22.5 Ω

for pristine PEDOT film. The low difference between these values indicates that the conductive matrix is mostly responsible for facile charge transfer.

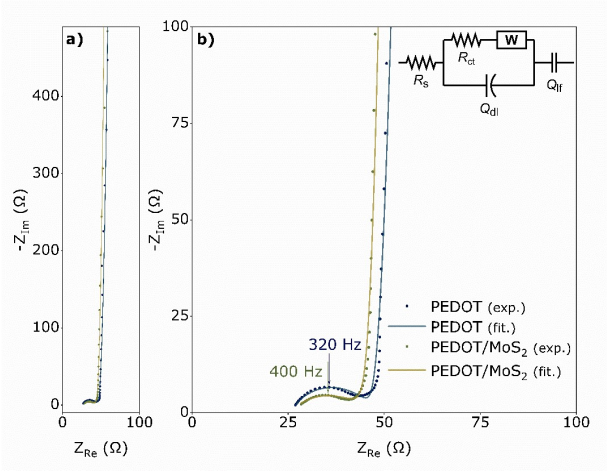

Figure 8. Electrochemical impedance spectra of PEDOT and PEDOT/MoS_2.

The comparison of values obtained in this work to those published previously (Table 1) allows to conclude that our reported values are promising in terms of areal capacitance, as they exceed the majority of available data on PEDOT/MoS_2 and similar materials, including those containing PEDOT:PSS copolymer and WS_2, which is structurally similar (both are two-dimensional layered materials) to MoS_2 and thus should provide the same charge storage mechanism. Notably, similar work [25] presents promising results with enhanced electrochemical properties, when the MoS_2 was synthesized instead of using commercially available option. This may be connected to the necessity of enhancing cycling stability of PEDOT/MoS_2 composite in our case, as ~0% loss per 1000 cycles is expected ideally. Aside from synthesis of more refined nanoparticles, this also may be achieved by limiting the potential window or using non-aqueous electrolytes, which would eliminate possible side reactions near the extremities of the potential window.

Table 1. Performance of analogous materials based on MoS_2, PEDOT, and WS_2.

Material	Capacitance, mF cm^{-2}	Stability (% of initial capacitance / cycles)	Electrolyte
MoS_2 (films) [42]	10–25	(87–101)/1000	1 mol dm^{-3} Na_2SO_4
MoS_2 (exfoliated) [43]	0.9–8.7	800/3000	1 mol dm^{-3} Na_2SO_4
MoS_2 (exfoliated) [44]	2.4	~80/200	Et_4NBF_4 in BMIM-PF_6
PEDOT(BF_4^-)/MoS_2 [13]	33–150	85/1000	1 mol dm^{-3} KCl
PEDOT(BF_4^-) [13]	7–39	—	1 mol dm^{-3} KCl
PEDOT:PSS/MoS_2 [21]	375	100/1000	PBS (pH = 7.4)
PEDOT:PSS/MoS_2 [24]	474	94/5000	1 mol dm^{-3} Na_2SO_4
PEDOT@MoS_2 [25]	2450	98.5/5000	1 mol dm^{-3} H_2SO_4
PEDOT-PEG-WS_2 [45]	186–237	91/5000	1 mol dm^{-3} H_2SO_4
PEDOT-PEG [45]	78	—	1 mol dm^{-3} H_2SO_4
WS_2/PEDOT:PSS [46]	61–79	107/5000	1 mol dm^{-3} H_2SO_4

PEDOT/MoS_2 (this work)	108–870	87/100, 71/350	1 mol dm^{-3} $LiClO_4$
PEDOT (this work)	80	—	1 mol dm^{-3} $LiClO_4$

4 Conclusions

The original method of PEDOT-matrix-assisted electrochemical synthesis of PEDOT/MoS_2 composite with finely dispersed MoS_2 particles spread over the volume of polymer film was proposed. The obtained exceptionally high capacitance values of composite (up to 870 mF cm^{-2} at 1 mA cm^{-2}) outperformed most earlier reported data on similar pseudocapacitive materials. The composite material is highly conductive, which allows to obtain thicker films, thus increasing areal capacitance. Voltammetric and charge-discharge data show that the materials can be easily obtained on carbon-based substrates both in galvanostatic and potentiodynamic modes of synthesis. The potentials windows above 1.1 V led to degradation of the polymer, and lower potentials areas (<-0.4 V) are unsuited for acidic (H_2SO_4) electrolytes. We established the possibility of using such material in KCl, Li_2SO_4, and $LiClO_4$ electrolytes, and redox response is most noticeable in Li_2SO_4 and KCl. The potentiostatically synthesized supercapacitor electrode materials provide up to 870 mF cm^{-2} at 1 mA cm^{-2} in asymmetric system with Kynol carbon cloth counter electrode, which is an exceptionally high capacitance. The cycling window of 1.7 V is optimal in $LiClO_4$ solution and could be further increased in organic electrolytes. The aqueous nature of electrolyte in our work may be a reason of 71% of initial capacitance retaining after 350 charge-discharge cycles, thus this material may be further increased by optimizing the system, i.e., limiting the potentials. The proposed approach can be further adapted as a prospective method of obtaining composite electrode materials.

Data availability

The raw and processed data required to reproduce these findings are available upon request addressed to corresponding author.

Acknowledgements

The authors would like to thank Centre for X-ray Diffraction Studies, Interdisciplinary Resource Centre for Nanotechnology, and Centre for Physical Methods of Surface Investigation of Research Park of St. Petersburg State University for XRD, SEM, EDX, TEM, and XPS studies.

Funding

The reported study was funded by Russian Foundation for Basic Research, project number 20-33-90143.

References

[1] W. Raza, F. Ali, N. Raza, Y. Luo, K.H. Kim, J. Yang, S. Kumar, A. Mehmood, E.E. Kwon, Recent advancements in supercapacitor technology, Nano Energy. 52 (2018) 441–473. doi:10.1016/j.nanoen.2018.08.013.

[2] J. Wu, F. Ciucci, J.K. Kim, Molybdenum Disulfide Based Nanomaterials for Rechargeable Batteries, Chem. - A Eur. J. 26 (2020) 6296–6319. doi:10.1002/chem.201905524.

[3] J.M. Soon, K.P. Loh, Electrochemical double-layer capacitance of MoS_2 nanowall films, Electrochem. Solid-State Lett. 10 (2007) 250–254. doi:10.1149/1.2778851.

[4] W.J. Zhang, K.J. Huang, A review of recent progress in molybdenum disulfide-based supercapacitors and batteries, Inorg. Chem. Front. 4 (2017) 1602–1620. doi:10.1039/c7qi00515f.

[5] X. Li, H. Zhu, Two-dimensional MoS_2: Properties, preparation, and applications, J. Mater. 1 (2015) 33–44. doi:10.1016/j.jmat.2015.03.003.

[6] E.G. Da Silveira Firmiano, A.C. Rabelo, C.J. Dalmaschio, A.N. Pinheiro, E.C. Pereira, W.H. Schreiner, E.R. Leite, Supercapacitor electrodes obtained by directly bonding 2D MoS_2 on reduced graphene oxide, Adv. Energy Mater. 4 (2014) 1301380. doi:10.1002/aenm.201301380.

[7] D. Sarkar, D. Das, S. Das, A. Kumar, S. Patil, K.K. Nanda, D.D. Sarma, A. Shukla, Expanding Interlayer Spacing in MoS_2 for Realizing an Advanced Supercapacitor, ACS Energy Lett. 4 (2019) 1602–1609. doi:10.1021/acsenergylett.9b00983.

[8] M. Acerce, D. Voiry, M. Chhowalla, Metallic 1T phase MoS_2 nanosheets as supercapacitor electrode materials, Nat. Nanotechnol. 10 (2015) 313–318. doi:10.1038/nnano.2015.40.

[9] Q. Mahmood, S.K. Park, K.D. Kwon, S.J. Chang, J.Y. Hong, G. Shen, Y.M. Jung, T.J. Park, S.W. Khang, W.S. Kim, J. Kong, H.S. Park, Transition from Diffusion-Controlled Intercalation into Extrinsically Pseudocapacitive Charge Storage of MoS_2 by Nanoscale Heterostructuring, Adv. Energy Mater. 6 (2016) 1501115. doi:10.1002/aenm.201501115.

[10] S. Patil, A. Harle, S. Sathaye, K. Patil, Development of a novel method to grow mono-/few-layered MoS_2 films and MoS_2-graphene hybrid films for supercapacitor applications, CrystEngComm. 16 (2014) 10845–10855. doi:10.1039/c4ce01595a.

[11] M. Li, A. Addad, Y. Zhang, A. Barras, P. Roussel, M.A. Amin, S. Szunerits, R. Boukherroub, Flower-like Nitrogen-co-doped MoS_2@RGO Composites with Excellent Stability for Supercapacitors, ChemElectroChem. 8 (2021)

2903–2911. doi:10.1002/celc.202100401.

[12] K.J. Huang, L. Wang, Y.J. Liu, H.B. Wang, Y.M. Liu, L.L. Wang, Synthesis of polyaniline/2-dimensional graphene analog MoS_2 composites for high-performance supercapacitor, Electrochim. Acta. 109 (2013) 587–594. doi:10.1016/j.electacta.2013.07.168.

[13] D. Li, D. Zhu, W. Zhou, Q. Zhou, T. Wang, G. Ye, L. Lv, J. Xu, Design and electrosynthesis of monolayered MoS_2 and BF_4^--doped poly(3,4-ethylenedioxythiophene) nanocomposites for enhanced supercapacitive performance, J. Electroanal. Chem. 801 (2017) 345–353. doi:10.1016/j.jelechem.2017.08.012.

[14] G. Ma, H. Peng, J. Mu, H. Huang, X. Zhou, Z. Lei, In situ intercalative polymerization of pyrrole in graphene analogue of MoS_2 as advanced electrode material in supercapacitor, J. Power Sources. 229 (2013) 72–78. doi:10.1016/j.jpowsour.2012.11.088.

[15] H. Tang, J. Wang, H. Yin, H. Zhao, D. Wang, Z. Tang, Growth of polypyrrole ultrathin films on MoS_2 monolayers as high-performance supercapacitor electrodes, Adv. Mater. 27 (2015) 1117–1123. doi:10.1002/adma.201404622.

[16] J. Wang, Z. Wu, H. Yin, W. Li, Y. Jiang, Poly(3,4-ethylenedioxythiophene)/MoS_2 nanocomposites with enhanced electrochemical capacitance performance, RSC Adv. 4 (2014) 56926–56932. doi:10.1039/c4ra12683a.

[17] A.V. Murugan, M. Quintin, M.H. Delville, G. Campet, C.S. Gopinath, K. Vijayamohanan, Exfoliation-induced nanoribbon formation of poly(3,4-ethylene dioxythiophene) PEDOT between MoS_2 layers as cathode material

for lithium batteries, J. Power Sources. 156 (2006) 615–619. doi:10.1016/j.jpowsour.2005.06.022.

[18] Y. Ge, R. Jalili, C. Wang, T. Zheng, Y. Chao, G.G. Wallace, A robust free-standing MoS_2/poly(3,4-ethylenedioxythiophene):poly(styrenesulfonate) film for supercapacitor applications, Electrochim. Acta. 235 (2017) 348–355. doi:10.1016/j.electacta.2017.03.069.

[19] A.V. Murugan, M. Quintin, M.H. Delville, G. Campet, A.K. Viswanath, C.S. Gopinath, K. Vijayamohanan, Synthesis and characterization of organic-inorganic poly(3,4-ethylenedioxythiophene)/MoS_2 nanocomposite via in situ oxidative polymerization, J. Mater. Res. 21 (2006) 112–118. doi:10.1557/jmr.2006.0015.

[20] T. Alamro, M.K. Ram, Polyethylenedioxythiophene and molybdenum disulfide nanocomposite electrodes for supercapacitor applications, Electrochim. Acta. 235 (2017) 623–631. doi:10.1016/j.electacta.2017.03.102.

[21] D.V.S.K. Gunapu, V.S. Mudigunda, A. Das, A.K. Rengan, S.R.K. Vanjari, Facile synthesis and characterization of Poly(3,4-ethylenedioxythiophene)/Molybdenum disulfide (PEDOT/MoS_2) composite coatings for potential neural electrode applications, J. Appl. Electrochem. 50 (2020) 943–958. doi:10.1007/s10800-020-01447-8.

[22] D.K. Bhat, M.S. Kumar, N and p doped poly(3,4-ethylenedioxythiophene) electrode materials for symmetric redox supercapacitors, J. Mater. Sci. 42 (2007) 8158–8162. doi:10.1007/s10853-007-1704-9.

[23] C. Peng, G.A. Snook, D.J. Fray, M.S.P. Shaffer, G.Z. Chen, Carbon nanotube stabilised emulsions for electrochemical synthesis of porous nanocomposite coatings of poly[3,4-ethylene-dioxythiophene], Chem. Commun. (2006)

4629–4631. doi:10.1039/b609293d.

[24] Y. Chao, Y. Ge, Z. Chen, X. Cui, C. Zhao, C. Wang, G.G. Wallace, One-Pot Hydrothermal Synthesis of Solution-Processable MoS_2/PEDOT:PSS Composites for High-Performance Supercapacitors, ACS Appl. Mater. Interfaces. 13 (2021) 7285–7296. doi:10.1021/acsami.0c21439.

[25] Y. Cai, L. Xu, H. Kang, W. Zhou, J. Xu, X. Duan, X. Lu, Q. Xu, Electrochemical self-assembled core/shell PEDOT@MoS_2 composite with ultra-high areal capacitance for supercapacitor, Electrochim. Acta. 370 (2021) 137791. doi:10.1016/j.electacta.2021.137791.

[26] A. Lewandowski, A. Olejniczak, M. Galinski, I. Stepniak, Performance of carbon-carbon supercapacitors based on organic, aqueous and ionic liquid electrolytes, J. Power Sources. 195 (2010) 5814–5819. doi:10.1016/j.jpowsour.2010.03.082.

[27] F. Crameri, G.E. Shephard, Scientific colour maps, Zenodo (2021). doi:10.5281/zenodo.4491293.

[28] F. Crameri, G.E. Shephard, P.J. Heron, The misuse of colour in science communication, Nat. Commun. 11 (2020) 5444. doi:10.1038/s41467-020-19160-7.

[29] V. V. Kondratiev, S.N. Eliseeva, E.G. Tolstopyatova, A.O. Nizhegorodova, Electrochemical cell for the synthesis of nanocomposite materials, RU149730U1, 2014.

[30] V. V. Kondratiev, S.N. Eliseeva, E.G. Tolstopjatova, A.O. Nizhegorodova, Method of nanocomposite materials production and device for its implementation, RU2568807C1, 2014.

[31] M.A. del Valle, A.M. Ramírez, L.A. Hernández, F. Armijo, F.R. Díaz, G.C. Arteaga, Influence of the supporting electrolyte on the electrochemical polymerization of 3,4-ethylenedioxythiophene. effect on p- and n-Doping/Undoping, Conductivity And Morphology, Int. J. Electrochem. Sci. 11 (2016) 7048–7065. doi:10.20964/2016.08.46.

[32] A.R. Hillman, S.J. Daisley, S. Bruckenstein, Ion and solvent transfers and trapping phenomena during n-doping of PEDOT films, Electrochim. Acta. 53 (2008) 3763–3771. doi:10.1016/j.electacta.2007.10.062.

[33] Y. Jiao, A.M. Hafez, D. Cao, A. Mukhopadhyay, Y. Ma, H. Zhu, Metallic MoS_2 for High Performance Energy Storage and Energy Conversion, Small. 14 (2018) 1800640. doi:10.1002/smll.201800640.

[34] P. Joensen, E.D. Crozier, N.A. Alberding, R.F. Frindt, A study of single-layer and restacked MoS_2 by X-ray diffraction and X-ray absorption spectroscopy, J. Phys. C Solid State Phys. 20 (1987) 4043–4053. doi:10.1088/0022-3719/20/26/009.

[35] A. Ambrosi, Z. Sofer, M. Pumera, Lithium intercalation compound dramatically influences the electrochemical properties of exfoliated MoS_2, Small. 11 (2015) 605–612. doi:10.1002/smll.201400401.

[36] X. Chia, A. Ambrosi, Z. Sofer, J. Luxa, M. Pumera, Catalytic and charge transfer properties of transition metal dichalcogenides arising from electrochemical pretreatment, ACS Nano. 9 (2015) 5164–5179. doi:10.1021/acsnano.5b00501.

[37] A.R. Hillman, S.J. Daisley, S. Bruckenstein, Kinetics and mechanism of the electrochemical p-doping of PEDOT, Electrochem. Commun. 9 (2007) 1316–1322. doi:10.1016/j.elecom.2007.01.009.

[38] M. Ujvári, J. Gubicza, V. Kondratiev, K.J. Szekeres, G.G. Láng, Morphological changes in electrochemically deposited poly(3,4-ethylenedioxythiophene) films during overoxidation, J. Solid State Electrochem. 19 (2015) 1247–1252. doi:10.1007/s10008-015-2746-6.

[39] M.A. Kamensky, S.N. Eliseeva, G. Láng, M. Ujvári, V. V. Kondratiev, Electrochemical Properties of Overoxidized Poly-3,4-Ethylenedioxythiophene, Russ. J. Electrochem. 54 (2018) 893–901. doi:10.1134/S1023193518130219.

[40] S. Patra, K. Barai, N. Munichandraiah, Scanning electron microscopy studies of PEDOT prepared by various electrochemical routes, Synth. Met. 158 (2008) 430–435. doi:10.1016/j.synthmet.2008.03.002.

[41] Y.P. Gao, K.J. Huang, X. Wu, Z.Q. Hou, Y.Y. Liu, MoS_2 nanosheets assembling three-dimensional nanospheres for enhanced-performance supercapacitor, J. Alloys Compd. 741 (2018) 174–181. doi:10.1016/j.jallcom.2018.01.110.

[42] B.D. Falola, T. Wiltowski, I.I. Suni, Electrodeposition of MoS_2 for Charge Storage in Electrochemical Supercapacitors , J. Electrochem. Soc. 163 (2016) D568–D574. doi:10.1149/2.0011610jes.

[43] M.A. Bissett, I.A. Kinloch, R.A.W. Dryfe, Characterization of MoS_2-Graphene Composites for High-Performance Coin Cell Supercapacitors, ACS Appl. Mater. Interfaces. 7 (2015) 17388–17398. doi:10.1021/acsami.5b04672.

[44] A. Winchester, S. Ghosh, S. Feng, A.L. Elias, T. Mallouk, M. Terrones, S. Talapatra, Electrochemical characterization of liquid phase exfoliated two-dimensional layers of molybdenum disulfide, ACS Appl. Mater. Interfaces. 6

(2014) 2125–2130. doi:10.1021/am4051316.

[45] A. Liang, Y. Zhang, F. Jiang, W. Zhou, J. Xu, J. Hou, Y. Wu, Y. Ding, X. Duan, Electrochemical Self-Assembly of a 3D Interpenetrating Porous Network PEDOT-PEG-WS_2 Nanocomposite for High-Efficient Energy Storage, J. Phys. Chem. C. 123 (2019) 25428–25436. doi:10.1021/acs.jpcc.9b05227.

[46] A. Liang, D. Li, W. Zhou, Y. Wu, G. Ye, J. Wu, Y. Chang, R. Wang, J. Xu, G. Nie, J. Hou, Y. Du, Robust flexible WS_2/PEDOT:PSS film for use in high-performance miniature supercapacitors, J. Electroanal. Chem. 824 (2018) 136–146. doi:10.1016/j.jelechem.2018.07.040.